A NEW APPLICATON METHOD FOR LYZENGA'S OPTICAL MODEL

Tatsuyuki Sagawa[a,*], Teruhisa Komatsu[a], Etienne Boisnier[a], Karim Ben Mustapha[b], Abdalla Hattour[b], Naoko Kosaka[c] and Sanae Miyazaki[c]

[a]Ocean Research Institute, The University of Tokyo, 1-15-1 Minamidai, Nakano-ku, Tokyo, 164-8639, Japan
[b]Institut National des Schinces et Technologies de la Mer, 2025 Salammbo, Tunis, Tunisie
[c]NTT DATA Corporation, 3-3-3, Toyosu, Koutou-ku, Tokyo, 135-6033, Japan

KEY WORDS: Mapping accuracy, IKONOS, Coastal area, Radiometric correction, Remote sensing, Seagrass,

ABSTRACT:

Improving mapping accuracy is of primary interest in satellite remote sensing, especially when dealing with coastal areas, as underwater mapping remains a challenge. Radiometric correction is a key driver for accuracy and this process is generally closely related to the Lyzenga's optical model, which tries to explain mathematically the relation between bottom surface reflectance and the radiance level measured by satellite sensor. In this study, we develop a new radiometric correction method for this widely used model. The radiometric correction based on the Lyzenga's depth-invariant index has so far been primarily used. However, its efficiency is highly limited in low transparency areas (Jerlov Water Type II to III). In order to overcome such a problem, we propose a new index: the reflectance index. The efficiency of the latter with reference to the traditional depth-invariant index was demonstrated through two case studies: the Gabes Gulf part located off Mahares (Tunisia, Jerlov Water Type II to III) and Funakoshi Bay (Japan; Jerlov Water Type II). In both cases, mapping accuracy was significantly increased. This result not only highlights the suitability of our method to deal with low transparency waters but also underlines once again the importance of radiance correction in the mapping process.

1. INTRODUCTION

In satellite remote sensing, radiometric correction is a key driver for mapping accuracy. Radiometric correction is defined by the Canada Center for Remote Sensing as the "*calibration of recorded variance values reflected from (or emitted by) the ground scene*". Whilst this step may be ignored in the mapping process, Mumby and Clark (2000) showed that its use improves significantly the accuracy of the result. Contrary to Mumby and Edwards (2000), we argue that 'water column correction' (i.e. removing light absorption and scattering effect) is part of the radiometric correction, as it deals with recorded value calibration as well.

So far, despite its positive effect on mapping acurracy, radiometric corrections including compensation for light attenuation effects in the water have not been frequently used in the scope of satellite remote sensing. For instance, in a literature review conducted in 1998, Mumby et al. reported that only 4% of the studies involving remote sensing for mapping coastal area had used radiometric correction for the image analysis processing.

Any radiometric correction method is closely related to an optical model that explains mathematically the relation between radiance level recorded by optical sensor and bottom surface reflectance using mathematical equations. Lyzenga (1978), through a simple equation ignoring reflection taking place within the water body, was one of the pioneers in trying to model this relation. His model is still considered as a canonical reference (Karpouzli et al., 2003). In this study, we focus on the application methods specifically developed for Lyzenga's model and that imply radiometric correction. As a radiometric correction, Lyzenga (1978, 1981) proposed the calculation of a 'depth-invariant index' based on ratios of reflectance values between bands. Mumby et al. (1998) highlighted the efficiency of such a method for satellite and airborne images but also mentioned a major limit: this technique is only suitable for high clarity waters (Jerlov Water Types I to II). In this study, we developed a bottom reflectance index capable of not only improving accuracy for Jerlov Water Types I to II but also dealing with low transparency waters (Jerlov Waters Type II to III).

In order to test the value of this new reflectance index, we compared its efficiency with the depth-invariant index in mapping two different marine areas: the area located off Mahares, in the Gulf of Gabes (South-East Tunisia) and Funakoshi Bay, located in the Sanriku coastal area (North-Eastern part of Japan). Moreover, in both cases, we selected IKONOS images, as Mumby and Edwards (2002) pointed out that the high spatial resolution of this American satellite is particularly adapted to marine environment mapping.

2. METHOD

In this study, we evaluate the respective efficiency of each correction index through mapping accuracy. In that purpose, we used a 2-step method (Figure 1). First, the two radiometric correction methods under scrutiny were applied separately to a similar satellite image. Second, both corrected images were classified via supervised classification.

2.1 Radiometric correction methods

In the scope of radiometric correction, each pixel value within the image (DN value) is converted into radiance value. In case of IKONOS, the following converting equation is generally

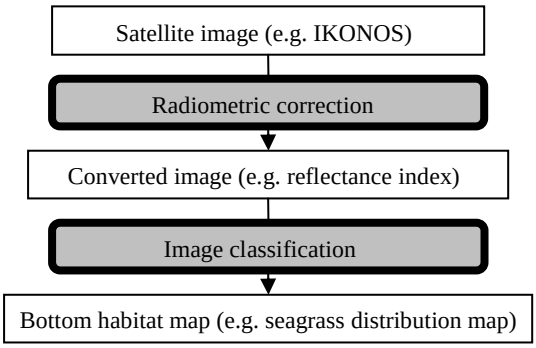

Figure 1 Image analysis process

used (Taylor, 2005):

$$L_i = \frac{DN_i}{CalCoef_i} \qquad (1)$$

where L_i = radiance in spectral band i at the sensor aperture (mW / cm^2 /str).
$CalCoef_i$ = in-band radiance calibration coefficient (cm^2 str / mW).
DN_i = image product value.

From an optical perspective, bottom type can be identified by its reflectance. According to Lyzenga (1978), the relationship between the radiance level recorded by optical sensor and bottom reflectance is expressed by the following equation:

$$L_i = L_{si} + a_i r_i \exp(-K_i g Z) \qquad (2)$$

where L_i = the radiance value calculated by equation (1).
L_{si} = the radiance recorded over deep water (external reflection from the water surface and scattering in the atmosphere).
a_i = a constant which includes the solar irradiance, the transmittance of the atmosphere and the water surface, and the reduction of the radiance due to refraction at the water surface (mW / cm^2 /str).
r_i = the bottom surface reflectance.
K_i = the effective attenuation coefficient of the water (m^{-1}).
g = a geometric factor to account for the path length through the water.
Z = the water depth (m).

Bottom differences are mirrored by variations in L_i, as r_i changes according to the bottom type. Radiometric Correction Index is required for estimating r_i and may be of two types: depth-invariant index or the one proposed by this study and named reflectance index.

2.2 Depth-invariant index

In order to remove light scattering and absorption effects within both atmosphere and water body, Lyzenga suggested the calculation of a depth-invariant index. This index is expressed as following:

$$Index_{ij} = \frac{K_j \ln(L_i - L_{si}) - K_i \ln(L_j - L_{sj})}{\sqrt{K_i^2 + K_j^2}} \qquad (3)$$

where L, L_s and K are the same as in equation (2). i and j correspond to satellite image bands.

Equation (3) is derived from equation (2) and refers simultaneously to 2 bands (band *i* and *j*). For calculating this index, ratios of attenuation coefficients between bands are necessary. In our case, these coefficients were obtained from sea truth data collected for sandy bottom along a depth gradient (Lyzenga, 1981). Side scan sonar measurements constitute a suitable tool for sea truth data collection (Sagawa et al., in press) and were used in this study.

2.3 The reflectance index proposed here (reflectance index)

In order to improve mapping accuracy, we propose an alternative radiometric correction. Our new reflectance index is expressed by the following equation:

$$Index_i = \frac{(L_i - L_{si})}{\exp(-K_i g Z)} \qquad (4)$$

where L, L_s, K, g and Z are similar to equation (2). i corresponds to a satellite image band.

To calculate this index, we need to combine depth data with attenuation coefficients. Each band attenuation coefficient was calculated by using the same sea truth data as for the depth-invariant index. Concerning depth data, we simply referred to the bathymetry map supplied by local government institutions. It looks reasonable to take advantage of these data, as they are easily available and represent generally a trustable input.
Once the numerator in equation (4) replaced by $a_i r_i \exp(-K_i g Z)$ (from equation (2)) and the equation rearranged, the index becomes the following equation including bottom reflectance:

$$Index_i = a_i r_i \qquad (5)$$

where a and r are the same as in equation (2). i corresponds to a satellite image band.

Clearly, this index is linearly related to bottom reflectance. As a result, we named it “reflectance index”. This index enables to compare not only the difference in reflectance ratios between bands but also the difference in absolute reflectance for each band.

2.4 Image Classification

Once the two radiometric correction types applied separately, the two different images obtained were classified by using the supervised classification based on maximum likelihood decision rule. At this step of the analysis, sea truth data concerning each bottom type distribution are required. These data were also collected using side scan sonar measurements.

According to Lyzenga (1978), equation (2) should not be applied to really shallow areas, as the model ignores internal reflection effects occurring at the water surface. As a result, in this study, we applied the above technique exclusively to area deeper than 2 m.

2.5 Evaluation of the technique

The marine area off Mahares and Funakoshi Bay were selected as test sites to evaluate the efficiency of the two radiometric correction methods. Mapping accuracy was calculating by using user accuracy, producer accuracy, overall accuracy (Congalton, 1991) and Tau coefficients (Ma and Redmond, 1995) derived from error matrixes. Here, we focus on Mahares case because this site is apparently more turbid than Funakoshi Bay and seems difficult for mapping.

On the 2nd October 2005, the corresponding IKONOS image was acquired. KONOS image has four bands (blue, green, red and infrared) but only two (blue and green) were used for classification, as light present in red and infrared wavelengths is rapidly absorbed by surface water layers. In this area, *Posidonia oceanica* is the most abundant and common species and it mainly occurs on sandy bottom. In this case, rather than distinguishing seagrass species, we tried to distinguish as accurately as possible *Posidonia oceanica* from sand. Respective reflectance for seagrass species and sand were measured via spectroradiometers (FieldSpec Pro, Analytical Spectral Devices Inc.). Field surveys were carried out from the 3rd to the 13th of November 2005.

We also conducted survey in Funakoshi Bay in similar method to Mahares.

3. RESULTS

In Mahares, attenuation coefficients estimated from sea truth data were respectively 0.088 m^{-1} for the blue band and 0.093 m^{-1} for the green band. Hence, according to Jerlov classification (Walker, 1994), Mahares belongs to Water Type II to III. Spectral reflectance for each bottom type is shown in figure 2. Sand and seagrass curves (*Posidonia oceanica*) are significantly different. The error matrixes are displayed in table 1 and indicate that mapping accuracy is increased when our reflectance index is used. A Z-test was conducted and underlined a significant difference of accuracy between tables 1(a) and 1(b) ($p < 0.05$). Similar statistical significance was recorded in Funakoshi Bay with regard to the accuracy improvement provided by our reflectance index.

4. DISCUSSION

Interestingly, Mumby et al. (2002) succeeded in getting relatively high user accuracy mapping (86-89 % for seagrass and 60-72 % for sand) by coupling depth invariant index and IKONOS image. It becomes then interesting to investigate why a similar method can lead to such variations in accuracy. We argue that differences are primarily linked with water transparency and turbidity levels.

First, Mumby reported extremely high water transparency

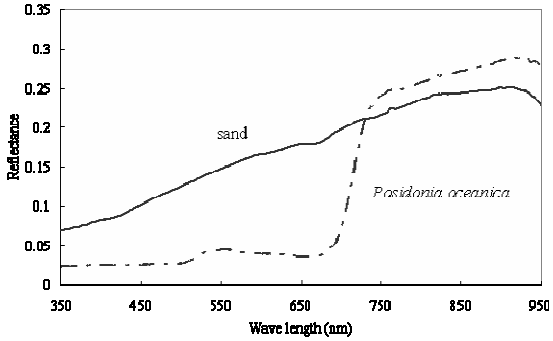

Figure 2 Reflectance level with reference to wavelength for each bottom feature (Mahares)

Table 1. Error matrixes for satellite image classification (Mahares)

(a) Error matrix obtained when using depth-invariant index

	Reference data			
Classification data	Seagrass	Sand	Row total	User accuracy
Seagrass	7	3	10	70.0%
Sand	43	47	90	52.2%
Column total	50	50	100	
Producer accuracy	14.0%	94.0%		
Overall accuracy	54.0%			
Tau coefficient	0.080			

(b) Error matrix obtained when using reflectance index

	Reference data			
Classification data	Seagrass	Sand	Row total	User accuracy
Seagrass	50	10	60	83.3%
Sand	0	40	40	100.0%
Column total	50	50	100	
Producer accuracy	100.0%	80.0%		
Overall accuracy	90.0%			
Tau coefficient	0.800			

(horizontal Secchi depth deeper than 50 m) in the scope of his study that took place off South Caicos, Turks and Caicos Islands (British West Indies). In Funakoshi Bay, according to Shibatani (2004), maximum Secchi depth equals 15 m while in Mahares, attenuation coefficients indicate that it may even be shallower. With regard to light penetration in water, these three sites are then highly different. Broadly speaking, due to sensor resolution limits, water transparency is an important variable to explain radiance level. Hence, when water transparency is high, radiance level recorded by satellite sensor is high as well, as attenuation within the water body is low. Moreover, when radiance level is high, distinctions between bottom types are made easier because boundaries between classes become clearer. Conversely, when radiance level decreases, these boundaries become blur and classification harder.

Second, despite the fact that red and infrared wavelength may contain useful data for distinguishing bottom types (figure 2), light contained in these two bands attenuates quickly in water such that they become useless when we have to deal with turbid

or deep waters. According to McCluney (1974), even in the case of high-clarity ocean water, penetration depth (i.e. the layer depth for which upwelling radiance equals 90% of its maximum value) is 3.8 m for the red band covering 600-700 nm. In a separate study, Green et al. (2000) noted that, at such a depth, the infrared (covering 800-1100 nm) is already completely absorbed.

What makes our method successful in low transparency conditions? Light attenuates not only in red and infrared bands but also in blue or green ones, even if the attenuation rate is much slower. Hence, the amount of light reflected at the bottom surface decreases as depth increases. As a result, as pointed out by Lyzenga (1978), mapping accuracy tends to drop, as water depth goes up. This 'depth effect' may be linked with solar irradiance level, water turbidity or even mapping method. As illustrated by figure 2, difference between absolute reflectance values for blue and green bands is large and the higher these differences are, the easier it is to identify bottom types and to increase general mapping accuracy. Our technique takes advantage of the sea chart bathymetry data available for almost any coastal area around the globe. Consequently, and this may appear as a potential drawback, bathymetry data accuracy is of primary concern. Though, the real influence of mistakes on the final mapping result remains unclear and will represent the object of a future study.

Pasqualini et al., (1998) also referred to bathymetry data in order to reduce attenuation effect within the water body but the rules driving their depth classification remains unclear. To be more precise, they divided the image according to three depth ranges (0 to 5 m, 5 to 10 m and 10 to 20 m) before conducting supervised classification. Authors explained this choice of depth ranges with reference to the map used. Nonetheless, we remain convinced that increasing bathymetry map accuracy (i.e. more depth gradients) is essential to really benefit from the accuracy improvement provided by depth data, even if it signifies increasing sampling *in situ* as well. As a result, with regard to Pasqualini et al., our method seems much less arguable.

This study shows that radiometric correction based on our reflectance index permits to map marine areas classified as Jerlov Water Type Ⅱ to Ⅲ with regard to their transparency. We hope these results will create incentives to apply more frequently radiometric correction.

5. ACKNOWLEDGEMENTS

We thank staffs from the International Coastal Research Center, the Ocean Research Institute, the University of Tokyo, and the Institut National des Sciences et Technologies de la Mer who helped us in situ and provided useful advices. We are also grateful to SEA Corporation and Oyo Corporation employees who were highly helpful for sonar measurements. Finally, we would like to thank Mr. Yoshikazu Ozeki from Japan Space Imaging Corporation as well for his cooperation. Our study was partially supported by a Research Fellowship Grant for Young Scientists from the Japanese Society for the Promotion of Science.

6. REFERENCES

Canada Center for Remote Sensing. http://www.ccrs.nrcan.gc.ca/ Accessed the 15th of May, 2007.

Congalton, R.G. (1991). A Review of Assessing the Accuracy of Classifications of Remotely Sensed Data. *Remote Sensing of Environment, 37*, 35-46.

Green, E., Edwards, A. and Mumby, P. (2000). Mapping. bathymetry. In A.J. Edwards (Ed.), *Remote sensing handbook for tropical coastal management* (pp.219-234). Paris: UNESCO.

Karpouzli, E., Malthus, T., Place, C., Chui, A.M., Garcia, M.I., and Mair, J. (2003). Underwater light characterisation for correction of remotely sensed images. *International Journal of Remote Sensing, 24*, 2683-2702.

Ma, Z.K., and Redmond, R.L. (1995). Tau-Coefficients for Accuracy Assessment of Classification of Remote-Sensing Data. *Photogrammetric Engineering and Remote Sensing, 61*, 435-439.

McCluney, W.R. (1974). Estimation of sun light penetration in the sea for remote sensing. *NASA Report, X-70643*.

Mumby, P.J., and Edwards, A.J. (2002). Mapping marine environments with IKONOS imagery: enhanced spatial resolution can deliver greater hematic accuracy. *Remote Sensing of Environment, 82*, 248-257.

Mumby, P. and Clark, C (2000). Radiometric correction of satellite and airborne images. In A.J. Edwards (Ed.), *Remote sensing handbook for tropical coastal management* (pp.109-120). Paris: UNESCO.

Mumby, P.J., Clark, C.D., Green, E.P., and Edwards, A.J. (1998). Benefits of water column correction and contextual editing for mapping coral reefs. *International Journal of Remote Sensing, 19*, 203-210.

Mumby, P.J. and Edwards, A.J. (2000). Water column correction techniques. In A.J. Edwards (Ed.), *Remote sensing handbook for tropical coastal management* (pp.121-128). Paris: UNESCO.

Lyzenga, D.R. (1978). Passive Remote-Sensing Techniques for Mapping Water Depth and Bottom Features. *Applied Optics*, **17**, 379-383.

Lyzenga, D.R. (1981) Remote sensing of bottom reflectance and water attenuation parameters in shallow water using aircraft and Landsat data. *International Journal of Remote Sensing*, **10**, 53-69.

Pasqualini, V., Pergent-Martini, C., Clabaut, P., and Pergent, G. (1998). Mapping of *Posidonia oceanica* using aerial

photographs and side scan sonar: Application off the Island of Corsica (France). *Estuarine Coastal and Shelf Science, 47*, 359-367.

Sagawa, T., Mikami, A., Komatsu, T., Kosaka, N., Kosako, A., Miyazaki, S. and Takahashi, M., in press, Mapping seagrass beds using IKONOS satellite image and side scan sonar measurements: a Japanese case study. *International journal of remote sensing.*

Shibatani, K. (2004). Distribution and environment of seagrass in Funakoshi Bay, Iwate Prefecture. *Master thesis, Ocean Environmental, Marine Biology and Biological Resources course, Graduate School of Frontier Sciences, The University of Tokyo*, (14 pp.).

Taylor, M. (2005). IKONOS planetary reflectance and mean solar exoatmospheric irradiance, IKONOS planetary reflectance QSOL Rev.1. Report available online (http://www.geoeye.com/products/imagery/ikonos/sp ctral.htm). Accessed the 15th of May 2007.

Walker, R.E. (1994). Marine light field statistics: Hydrologic optics, New York: John Wiley and Sons, Inc., pp.136-198.